Progress In Electromagnetics Research B, Vol. 17, 101–116, 2009

A UAPO-BASED MODEL FOR PROPAGATION PREDICTION IN MICROCELLULAR ENVIRONMENTS

G. Gennarelli and G. Riccio

Dipartimento di Ingegneria dell' Informazione ed Ingegneria Elettrica
Università di Salerno via Ponte Don Melillo
I-84084 Fisciano (SA), Italy

Abstract—A propagation model is presented in this paper for predicting the field strength in microcellular environments. According to the Geometrical Theory of Diffraction, the total field at a given observation point is calculated by summing the Geometrical Optics contributions and the field diffracted by the edges of each structure. The diffraction contributions are here evaluated by means of a Uniform Asymptotic Physical Optics solution to the corresponding canonical problem. Such a solution, expressed in terms of the standard transition function of the Uniform Theory of Diffraction, has resulted to be able to compensate the Geometrical Optics discontinuities at the shadow boundaries. In this framework, the structures are treated as constituted by lossy dielectric materials assumed to be non penetrable. The effectiveness of the here proposed model has been tested in some typical scenarios by means of comparisons with the Finite Difference Time Domain method.

1. INTRODUCTION

The knowledge of the propagation characteristics is a basic step in the design of mobile radio communication systems. As well-known, the propagation prediction based on ray-tracing has emerged as the most successful technique in the case of microcellular radio networks, where base station antennas are usually positioned below the rooftop height of the surrounding buildings in order to constrain the radio coverage to a small number of roads. In this framework, due to the analytic representation of the electromagnetic field as a complex vector, the ray-based models provide detailed characterization of the channel and allow

Corresponding author: G. Riccio (riccio@diiie.unisa.it).

one to calculate magnitude and phase of the received field, and the delay of each ray component arriving at the receiver after undergoing propagation mechanisms. These last are complex and diverse, and can generally be attributed to reflection, diffraction, and scattering.

The research activity on propagation mechanisms in urban microcell has been mainly focused on the modelling of reflection and diffraction from the exterior walls and corners of buildings, usually considered opaque. Several models [1–6] have been recently developed for estimating the field strength in two- or three-dimensional urban scenarios by explicitly considering the edge diffraction terms. They are based on the Geometrical Theory of Diffraction (GTD) for perfectly conducting structures, first proposed by Keller [7], improved by Kouyoumjian and Pathak [8] for removing the inaccuracies close to the incident and reflection boundaries, and subsequently extended by Luebbers [9] to finite conductivity wedges in heuristic way. The solution proposed by Luebbers for the diffracted field is easy to handle and to implement in ray-tracing tools. Despite its large use for solving practical propagation problems, it must be stressed that it does not possess a rigorous analytical and physical justification, and therefore it should be used only with considerable attention.

The aim of this paper is to propose an alternative propagation model for predicting the field strength in microcellular environments. It is based on a Uniform Asymptotic Physical Optics (UAPO) solution for the field diffracted by corners, assumed non-penetrable and with finite conductivity. In particular, the UAPO solution proposed in [10] is here extended to the three-dimensional case. The key point to do this is the use of a PO approximation of the equivalent surface currents induced by the incident field on the structure and of a uniform asymptotic evaluation of the resulting radiation integral. The final expression is in closed form and given in terms of the transition function of the Uniform Theory of Diffraction (UTD) [8]. It is easy to handle and to implement in ray-tracing tools like that developed in [9]. In addition, even if approximate, it relies on a sound theoretical basis, unlike that in [9].

The paper is organized as follows. The three-dimensional canonical problem involving a lossy dielectric wedge with arbitrary angle is described in Section 2. Some numerical examples are also reported to show the effectiveness of the UAPO diffracted field for compensating the GO field discontinuities at the shadow boundaries. The UAPO-based model is then applied in Section 3 to solve radio propagation in two real microcellular scenarios, and validated by means of comparisons with the Finite-difference Time-domain (FDTD) method [11]. Concluding remarks are reported in Section 4.

2. FINITE CONDUCTIVITY WEDGE: A UAPO-BASED SOLUTION

Let us consider the incidence of an arbitrarily polarized plane wave on a finite conductivity wedge, which is considered opaque, infinite in extension and surrounded by free-space (Fig. 1). The wedge has complex relative permittivity $\varepsilon_r = (\varepsilon - j\sigma/\omega)/\varepsilon_0$, relative permeability $\mu_r = 1$, and interior angle $\gamma = (2-n)\,\pi$. The incidence direction is fixed by the angles (β', ϕ'). In particular, β' is a measure of the incidence direction skewness with respect to the edge ($\beta' = \pi/2$ corresponds to the normal incidence). The observation direction is specified by (β, ϕ). The reference coordinate system has the z-axis directed along the edge and the x-axis on the upper surface S_0, so that this last corresponds to the zero value of the angles ϕ' and ϕ.

According to the GTD formulation, the total electric field at a given observation point external to the wedge can be expressed as sum of the GO field ($\underline{E}^{GO}$) and the field diffracted ($\underline{E}^{d}$) by the edge. For the considered canonical problem, the GO field includes the incident field and the field reflected from S_0 and S_n (the face at $\phi = n\,\pi$) with the edge ignored, namely,

$$\underline{E}^{GO} = \underline{E}^{i} u^{i} + \underline{E}_0^{r} u_0^{r} + \underline{E}_n^{r} u_n^{r} \tag{1}$$

wherein u^i, u_0^r, and u_n^r are unit step functions equal to the unity in the regions illuminated by the incident and reflected fields, and to zero in their shadow regions.

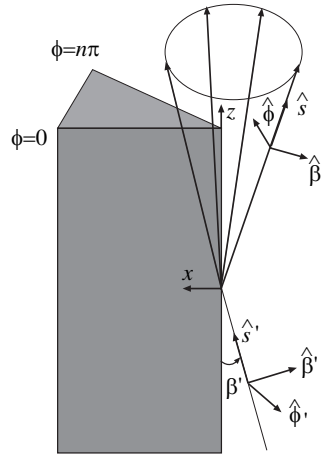

Figure 1. Geometry of the canonical problem.

The incident electric field can be expressed as:

$$\begin{aligned}\underline{E}^i &= \begin{pmatrix} E^i_\beta \\ E^i_\phi \end{pmatrix} e^{jk_0\rho\sin\beta'\cos(\phi-\phi')} e^{-jk_0 z\cos\beta'} \\ &= \underline{\underline{T}}^i \begin{pmatrix} E^i_{\beta'} \\ E^i_{\phi'} \end{pmatrix} e^{jk_0\rho\sin\beta'\cos(\phi-\phi')} e^{-jk_0 z\cos\beta'} \end{aligned} \tag{2}$$

where k_0 is the free-space wave-number, $E^i_{\beta'}$ and $E^i_{\phi'}$ are the field components (at the origin) along $\hat{\beta}' = \hat{\phi}' \times \hat{s}'$ and $\hat{\phi}' = (\hat{s}' \times \hat{z})/|\hat{s}' \times \hat{z}|$, respectively, $\hat{s}'$ being the unit vector in the incidence direction (see Fig. 1). The matrix $\underline{\underline{T}}^i$ relates the basis $\hat{\beta}', \hat{\phi}'$ to $\hat{\beta}, \hat{\phi}$, where $\hat{\beta} = \hat{\phi} \times \hat{s}$ and $\hat{\phi} = (\hat{s} \times \hat{z})/|\hat{s} \times \hat{z}|$, $\hat{s}$ being the unit vector in the diffraction direction, and is given by:

$$\underline{\underline{T}}^i = \begin{pmatrix} \cos^2\beta'\cos(\phi-\phi') - \sin^2\beta' & \cos\beta'\sin(\phi-\phi') \\ -\cos\beta'\sin(\phi-\phi') & \cos(\phi-\phi') \end{pmatrix} \tag{3}$$

The field reflected from the wedge surfaces can be conveniently evaluated by means of the reflection matrices $\underline{\underline{R}}^0$ and $\underline{\underline{R}}^n$ related to the ordinary planes of incidence for S_0 and S_n. For what concerns the reflection from S_0, the following relation holds:

$$\begin{aligned}\underline{E}^r_0 &= \begin{pmatrix} E^r_\beta \\ E^r_\phi \end{pmatrix} e^{jk_0\rho\sin\beta'\cos(\phi+\phi')} e^{-jk_0 z\cos\beta'} \\ &= \underline{\underline{T}}^{r_o}\,\underline{\underline{R}}^0\,\underline{\underline{T}}^{r_i} \begin{pmatrix} E^i_{\beta'} \\ E^i_{\phi'} \end{pmatrix} e^{jk_0\rho\sin\beta'\cos(\phi+\phi')} e^{-jk_0 z\cos\beta'} \end{aligned} \tag{4}$$

The reflection matrix $\underline{\underline{R}}^0$ is:

$$\underline{\underline{R}}^0 = \begin{pmatrix} R_\parallel & 0 \\ 0 & R_\perp \end{pmatrix} \tag{5}$$

wherein

$$R_\perp = \frac{\cos\theta^i - \sqrt{\varepsilon_r - \sin^2\theta^i}}{\cos\theta^i + \sqrt{\varepsilon_r - \sin^2\theta^i}} \tag{6}$$

$$R_\parallel = \frac{\varepsilon_r\cos\theta^i - \sqrt{\varepsilon_r - \sin^2\theta^i}}{\varepsilon_r\cos\theta^i + \sqrt{\varepsilon_r - \sin^2\theta^i}} \tag{7}$$

are the standard Fresnel's coefficients for both perpendicular and parallel polarization and θ^i is the incidence angle (see Fig. 2). The

matrices $\underline{\underline{T}}^{r_i}$ and $\underline{\underline{T}}^{r_o}$ are reported in the following:

$$\underline{\underline{T}}^{r_i} = \frac{1}{\sqrt{1-\sin^2\beta'\sin^2\phi'}} \begin{pmatrix} \cos\beta'\sin\phi' & \cos\phi' \\ -\cos\phi' & \cos\beta'\sin\phi' \end{pmatrix} \quad (8)$$

$$\underline{\underline{T}}^{r_o} = \frac{1}{\sqrt{1-\sin^2\beta'\sin^2\phi'}} \begin{pmatrix} T_{11}^{r_o} & T_{12}^{r_o} \\ T_{21}^{r_o} & T_{22}^{r_o} \end{pmatrix} \quad (9)$$

in which

$$\begin{aligned} T_{11}^{r_o} &= \cos\beta'\left\{\sin\phi + \sin^2\beta'\sin\phi'\left[1+\cos\left(\phi+\phi'\right)\right]\right\} \\ T_{12}^{r_o} &= \sin^2\beta'\cos\phi' - \cos^2\beta'\cos\phi \\ T_{21}^{r_o} &= \cos\phi - \sin^2\beta'\sin\phi'\sin(\phi+\phi') \\ T_{22}^{r_o} &= \cos\beta'\sin\phi \end{aligned}$$

The field reflected by S_n can be obtained in a similar way.

The starting point for determining the diffracted field is to consider a PO approximation for the electric and magnetic equivalent surface currents induced by the incident field. In the far-field approximation, the field generated by these currents on the wedge can be expressed by means of the well-known radiation integral:

$$\underline{E}^s \cong \underline{E}_0 + \underline{E}_n = -jk_0 \iint_S \left[\left(\underline{\underline{I}} - \hat{R}\hat{R}\right)\left(\zeta_0 \underline{J}_s^{PO}\right) + \underline{J}_{ms}^{PO} \times \hat{R}\right] G\left(\underline{r}, \underline{r}'\right) dS \quad (10)$$

where $S = S_0 + S_n$, $G(\underline{r}, \underline{r}') = e^{-jk_0|\underline{r}-\underline{r}'|} \Big/ (4\pi\,|\underline{r}-\underline{r}'|\,)$, ζ_0 is the free-space impedance, $\underline{r}$ and $\underline{r}'$ denote the observation and source points, respectively, $\hat{R}$ is the unit vector from the radiating element at $\underline{r}'$ to the observation point, and $\underline{\underline{I}}$ is the (3×3) identity matrix. Since the two field contributions can be formally derived in a similar way, only $\underline{E}_0$ is explicitly considered. With reference to this contribution, the electric and magnetic PO currents can be expressed in terms of the GO response of the structure as follows:

$$\begin{aligned} \zeta_0 \underline{J}_s^{PO} &= \zeta_0 \widetilde{\underline{J}}_s^{PO} e^{jk_0(x\sin\beta'\cos\phi' - z\cos\beta')} \\ &= \left[\left(1-R_\perp\right) E_\perp^i \cos\theta^i \hat{e}_\perp + \left(1+R_\parallel\right) E_\parallel^i \hat{t}\right] \cdot e^{jk_0(x\sin\beta'\cos\phi' - z\cos\beta')} \quad (11) \\ \underline{J}_{ms}^{PO} &= \widetilde{\underline{J}}_{ms}^{PO} e^{jk_0(x\sin\beta'\cos\phi' - z\cos\beta')} \\ &= \left[\left(1-R_\parallel\right) E_\parallel^i \cos\theta^i \hat{e}_\perp - \left(1+R_\perp\right) E_\perp^i \hat{t}\right] \cdot e^{jk_0(x\sin\beta'\cos\phi' - z\cos\beta')} \quad (12) \end{aligned}$$

where (x, z) are the coordinates of the integration point on the surface, $E_\parallel^i$ and $E_\perp^i$ are the field components along $\hat{e}_\parallel^i$ *and* $\hat{e}_\perp$ (see Fig. 2), and $\hat{t} = \hat{n} \times \hat{e}_\perp$.

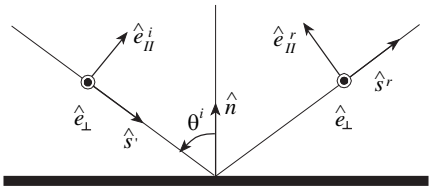

Figure 2. Ordinary plane of incidence.

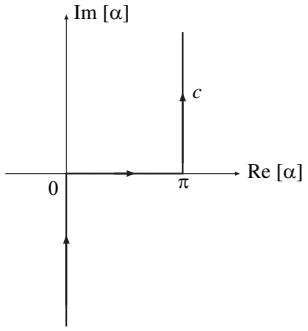

Figure 3. Integration path C in the complex α-plane.

As well-known, in the high-frequency approximation, the PO integral extended to S_0 can be reduced asymptotically to a sum of ray field contributions from (isolated) interior stationary phase points on S_0 and an edge diffracted field contribution. Moreover, since the diffraction is confined to the Keller's cone for which $\beta = \beta'$, the use of the approximation $\hat{R} = \hat{s}$ is permitted for evaluating the edge diffracted field [12]. Accordingly, it results:

$$\underline{E}_0 \cong \left[\left(\underline{\underline{I}} - \hat{s}\hat{s} \right) \left(\zeta_0 \underline{\tilde{J}}^{PO}_s \right) + \underline{\tilde{J}}^{PO}_{ms} \times \hat{s} \right] I_0 \tag{13}$$

where

$$\begin{aligned} I_0 &= -jk_0 \int_0^{+\infty} \int_{-\infty}^{+\infty} e^{jk_0(x \sin\beta' \cos\phi' - z\cos\beta')} G(\underline{r}, \underline{r}') \mathrm{d}z \, \mathrm{d}x \\ &= \frac{e^{-jk_0 z \cos\beta'}}{2(2\pi j)\sin\beta'} \int_C \frac{e^{-jk_0 x \sin\beta' \cos(\alpha \mp \phi)}}{\cos\alpha + \cos\phi'} d\alpha \end{aligned} \tag{14}$$

C being an appropriate integration path in the complex α-plane (see Fig. 3).

By applying the Cauchy's theorem, the contribution to the field related to the integration along C (distorted for the presence of singularities in the integrand) is equivalent to the summation of the integral along the Steepest Descent Path (SDP), passing through the pertinent saddle-point, and the residue contributions associated with all those poles that are inside the closed path C+SDP. A uniform asymptotic evaluation of the integral along the SDP provides the

UAPO edge diffraction contribution $\underline{E}_0^d$ in terms of the UTD transition function $F_t(\cdot)$ [8]:

$$\underline{E}_0^d = \underline{\underline{D}}_0 \begin{pmatrix} E_{\beta'}^i \\ E_{\phi'}^i \end{pmatrix} A(s) e^{-jk_0 s} \tag{15}$$

wherein s denotes the distance from the diffraction point to the observation point, $A(s) = 1/\sqrt{s}$ and

$$\underline{\underline{D}}_0 = \frac{e^{-j\pi/4}}{2\sqrt{2\pi k_0}\sin^2\beta'} \frac{F_t\left(k_0 L a\left(\phi \pm \phi'\right)\right)}{\cos\phi + \cos\phi'} \underline{\underline{T}}_0 u_0^d \tag{16}$$

In (16), u_0^d is the unit step function equal to 1 or 0 depending on the fact that S_0 is illuminated or not by the incident field, $a(x) = 2\cos^2(x/2)$ and $L = s\sin^2\beta'$. The sign + (−) applies if $0 < \phi < \pi$ ($\pi < \phi < n\pi$).

The contribution $\underline{E}_n^d$ related to S_n can be evaluated in a similar way, so obtaining:

$$\begin{aligned} \underline{E}^d &= \underline{E}_0^d + \underline{E}_n^d = \begin{pmatrix} E_\beta^d \\ E_\phi^d \end{pmatrix} = \underline{\underline{D}} \begin{pmatrix} E_{\beta'}^i \\ E_{\phi'}^i \end{pmatrix} A(s) e^{-jk_0 s} \\ &= \left(\underline{\underline{D}}_0 + \underline{\underline{D}}_n\right) \begin{pmatrix} E_{\beta'}^i \\ E_{\phi'}^i \end{pmatrix} A(s) e^{-jk_0 s} \end{aligned} \tag{17}$$

with

$$\underline{\underline{D}}_n = \frac{e^{-j\pi/4}}{2\sqrt{2\pi k_0}\sin^2\beta'} \frac{F_t\left[kLa((n\pi - \phi) \pm (n\pi - \phi'))\right]}{\cos(n\pi - \phi) + \cos(n\pi - \phi')} \underline{\underline{T}}_n u_n^d \tag{18}$$

The sign + (−) in (18) applies if $(n-1)\,\pi < \phi < n\,\pi$ ($0 < \phi < (n-1)\,\pi$). The explicit expressions of the matrices $\underline{\underline{T}}_0$ and $\underline{\underline{T}}_n$ are reported in Appendix.

In a real propagation scenario, radio waves have a spherical wave front. Consequently, the parameter L and the spreading factor $A(s)$ to be used must be changed according to [8].

Some numerical examples are reported in the following to test the effectiveness of the proposed approach. They refer to a lossy dielectric wedge characterized by $\varepsilon = 5\varepsilon_0$ and $\sigma = 0.01\,\mathrm{S/m}$. The working frequency is set to 2.4 GHz and the field is evaluated over a circular path with radius $10\lambda_0$, λ_0 being the free-space wavelength.

Numerical results reported in Figs. 4–6 refer to a wedge with $\gamma = 60°$. The incidence direction is $\beta' = 45°$, $\phi' = 60°$. The incident field is assumed to have only the β' component ($E_{\beta'}^i = 1$, $E_{\phi'}^i = 0$) and

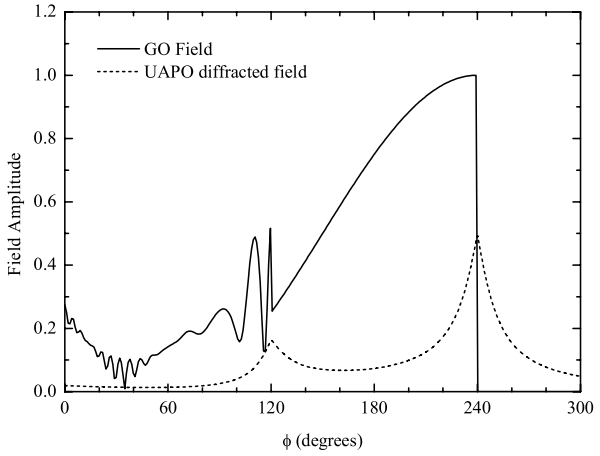

Figure 4. Amplitudes of the β – component of the GO response and the UAPO diffracted field contribution.

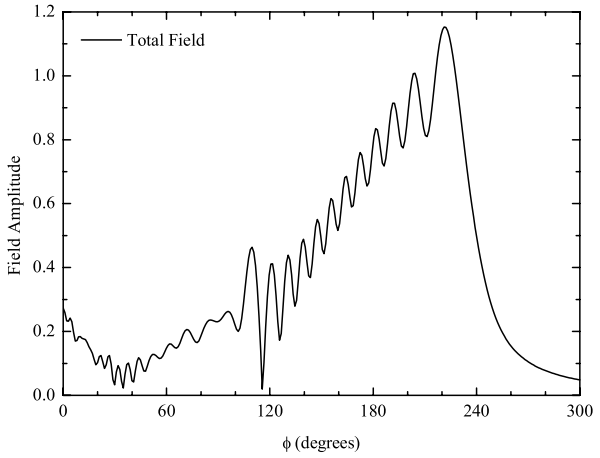

Figure 5. Amplitude of the β – component of the total field.

illuminates only the face S_0. As a consequence, only the diffraction contribution from its edge must be evaluated. The amplitudes of the electric field β — component related to the GO response and to the UAPO diffracted field contribution are reported in Fig. 4. As can be seen, the GO pattern has two discontinuities in correspondence of the reflection and incident shadow boundaries at $\phi = 120°$ and $\phi = 240°$. Furthermore, as expected, the UAPO diffracted field is not negligible in

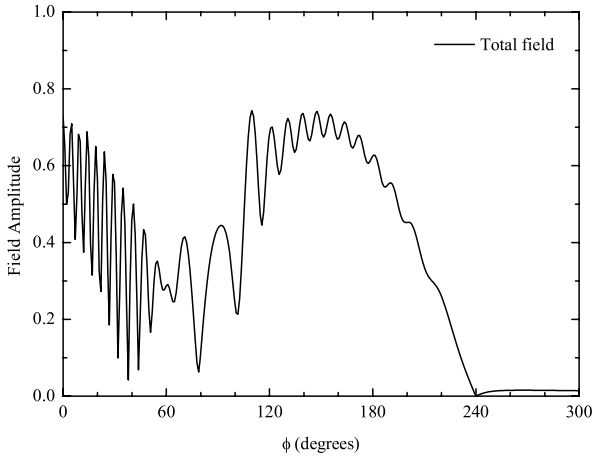

Figure 6. Amplitude of the ϕ — component of the total field.

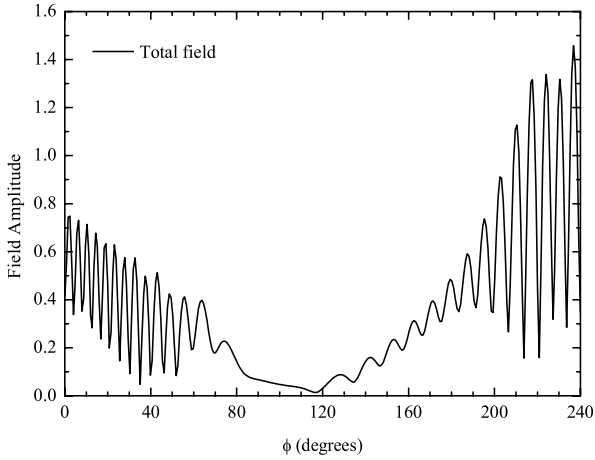

Figure 7. Amplitude of the β — component of the total field.

the neighbourhood of such boundaries. This guarantees the continuity of the total field (see Fig. 5). As expected, also the ϕ — component of the total field, reported in Fig. 6, is always continuous.

Results in Fig. 7 refer to a wedge with $\gamma = 120^\circ$ when illuminated according to the direction $\beta' = 45^\circ$, $\phi' = 120^\circ$. In this case, both faces of the wedge are illuminated by the incident field and generate a contribution to the total diffracted field. The results still confirm that the UAPO diffracted field solution perfectly compensates the GO field discontinuities.

3. TEST-BED PROPAGATION SCENARIOS

The UAPO-based propagation model described in the previous section is now employed to predict the field strength in two propagation scenarios and compared with the FDTD technique. The analysis here presented is only limited to the two dimensional case for saving time and computer resources.

Both transmitting and receiving antennas are assumed to be vertically polarized, so scalar problems can be tackled.

The first propagation case is relevant to a street canyon entrance. The geometry of the considered radio propagation environment is depicted in Fig. 8. The corners of the street are located at distances $d_1 = 4.24\,\mathrm{m}$ and $d_2 = 8.54\,\mathrm{m}$ from the transmitter Tx. The incidence direction on the wedges is specified by the angles $\phi'_1 = 45°$ and $\phi'_2 = 110.6°$, and the receiver moves along the track AB. The working frequency is set to 900 MHz and the buildings are characterized by $\varepsilon = 5\varepsilon_0$ and $\sigma = 0.01\,\mathrm{S/m}$. The street width is equal to 5 m and the observation track is located at its centre. For what concerns the GO field contributions, no more than two reflections are considered in the non line-of-sight region and a single reflection of the field diffracted is taken into account.

A FDTD code based on the Yee algorithm [13] has been developed in order to have a reference solution. The number of used cell per wavelength is 15. A Uniaxial Perfectly Matched Layer (UPML) [14] backed with a PEC wall is employed to bound the computational domain.

Figure 9 shows the amplitude of the GO response and the amplitudes of the diffracted field evaluated by means of the UAPO

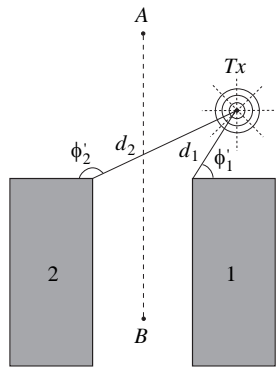

Figure 8. Propagation at a street canyon entrance.

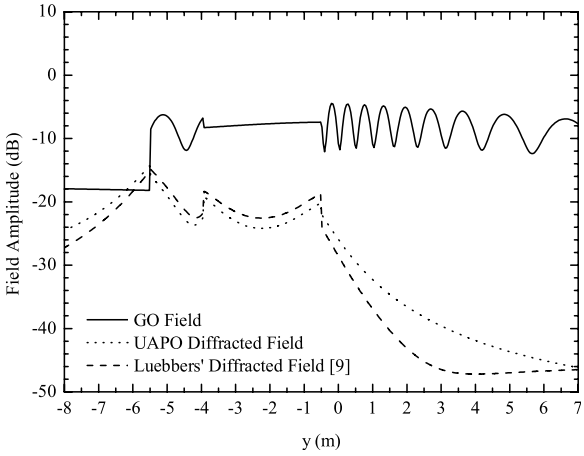

Figure 9. Propagation at a street canyon entrance: GO field, UAPO and Luebbers' diffracted field.

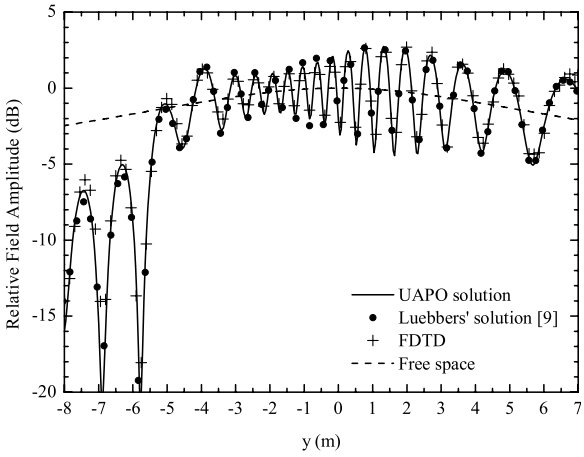

Figure 10. Propagation at a street canyon entrance: Total field.

solution and the Luebbers' solution. For what concerns the GO field, it exhibits three discontinuities. By moving from A to B, they are related to the boundary of the field reflected from the exterior face of the wedge 1, the boundary of the field reflected from the interior face of the wedge 2, and the boundary of the incident field. It is apparent that the UAPO and Luebbers' solutions for the diffracted field are comparable especially in proximity of the GO field shadow boundaries.

The relative amplitude of the total field is reported in Fig. 10. The free-space field is also represented to illustrate the attenuation produced by the building walls and its maximum is here assumed as normalization value. As expected, the UAPO diffracted field perfectly compensates the GO field discontinuities. In addition, the good agreement attained with the FDTD results validates its accuracy and effectiveness.

The second example considered as test-bed is relevant to a crossroads with the presence of two buildings (see Fig. 11). The frequency and the electromagnetic parameters of the buildings are the same used in the previous example. In addition, $d_1 = 5.66\,\mathrm{m}$, $d_2 = 9.05\,\mathrm{m}$, $\phi'_1 = 45°$, $\phi'_2 = 83.7°$.

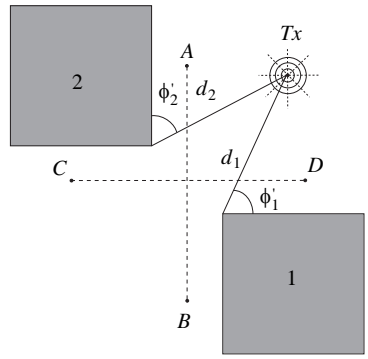

Figure 11. Propagation at a crossroads.

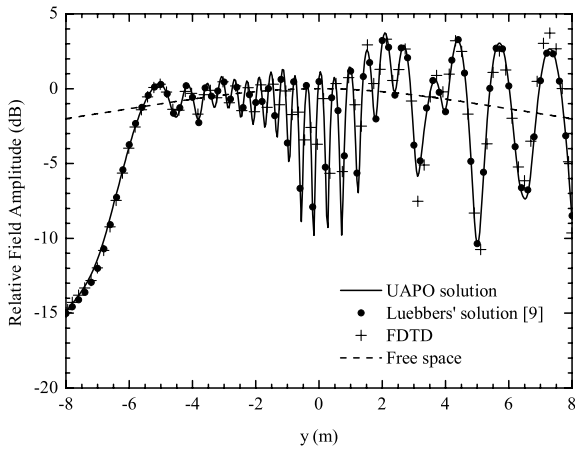

Figure 12. Propagation at a crossroads: Total field along the track AB.

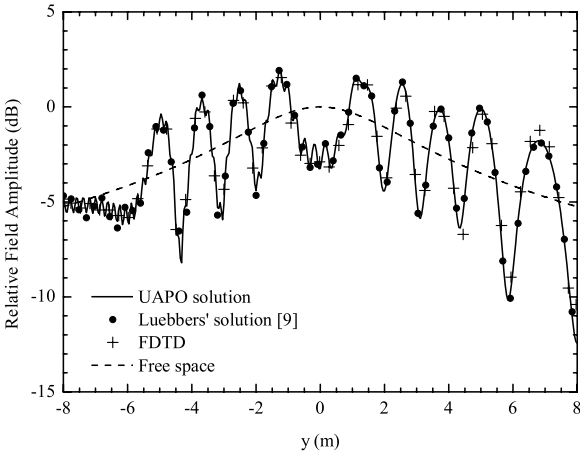

Figure 13. Propagation at a crossroads: Total field along the track CD.

The receiver moves along two perpendicular paths. In particular, the track AB is 2.5 m far from buildings 1 and 2, whereas the track CD is 1.5 m far from buildings 1 and 2.

The field levels along the tracks AB and CD are shown in Figs. 12 and 13. As can be seen, both the comparisons with the FDTD results confirm the accuracy of the proposed UAPO-based model once again.

4. CONCLUSIONS

A model for predicting the propagation in microcellular environments has been presented in this paper. It is based on the UAPO solution for the field diffracted by a non-penetrable lossy wedge illuminated at oblique incidence. The expression of the diffracted field is here derived in closed form and given in terms of the UTD transition function [8]. It is easy to handle and to implement in ray-tracing tools like that developed in [9]. Moreover, it relies on a sound theoretical basis, unlike that in [9], and can be extended to penetrable wedges as future work.

The analysis carried out in this work suggests that the proposed UAPO-based model is reliable and accurate in making field level predictions and can be surely applied to complex three-dimensional radio propagation problems.

APPENDIX A.

The expressions of the matrices $\underline{\underline{T}}_0$ and $\underline{\underline{T}}_n$ involved in the UAPO solution for the diffraction coefficients (16), (18) are made explicit.

For what concerns $\underline{\underline{T}}_0$, it can be expressed as follows:

$$\underline{\underline{T}}_0 = \underline{\underline{T}}_1 \left[\underline{\underline{T}}^0_2 \underline{\underline{T}}^0_4 \underline{\underline{T}}^0_5 + \underline{\underline{T}}^0_3 \underline{\underline{T}}^0_4 \underline{\underline{T}}^0_6 \right] \underline{\underline{T}}^0_7 \tag{A1}$$

where

$$\underline{\underline{T}}_1 = \begin{pmatrix} \cos\beta' \cos\phi & \cos\beta' \sin\phi & -\sin\beta' \\ -\sin\phi & \cos\phi & 0 \end{pmatrix} \tag{A2}$$

is the transformation matrix for the edge- to ray-fixed coordinate system components,

$$\underline{\underline{T}}^0_4 = \frac{1}{\sqrt{1 - \sin^2\beta' \sin^2\phi'}} \begin{pmatrix} -\cos\beta' & -\sin\beta' \cos\phi' \\ -\sin\beta' \cos\phi' & \cos\beta' \end{pmatrix} \tag{A3}$$

is the transformation matrix relating the base $\hat{e}_{\perp,0}$, $\hat{t}_0$ to $\hat{x}$, $\hat{z}$;

$$\underline{\underline{T}}^0_7 = \frac{1}{\sqrt{1 - \sin^2\beta' \sin^2\phi'}} \begin{pmatrix} \cos\beta' \sin\phi' & \cos\phi' \\ -\cos\phi' & \cos\beta' \sin\phi' \end{pmatrix} \tag{A4}$$

relates the base $\hat{\beta}', \hat{\phi}'$ to $\hat{e}^i_{\parallel,0}$, $\hat{e}^i_{\perp,0}$ in the plane normal to the incidence direction and, at last,

$$\underline{\underline{T}}^0_2 = \begin{pmatrix} 1 - \sin^2\beta' \cos^2\phi & -\cos\beta' \sin\beta' \cos\phi \\ -\sin^2\beta' \sin\phi \cos\phi & -\cos\beta' \sin\beta' \sin\phi \\ -\cos\beta' \sin\beta' \cos\phi & \sin^2\beta' \end{pmatrix} \tag{A5}$$

$$\underline{\underline{T}}^0_3 = \begin{pmatrix} 0 & -\sin\beta' \sin\phi \\ -\cos\beta' & \sin\beta' \cos\phi \\ \sin\beta' \sin\phi & 0 \end{pmatrix} \tag{A6}$$

$$\underline{\underline{T}}^0_5 = \begin{pmatrix} 0 & \left[1 - R^0_\perp\right] \cos\theta^i_0 \\ 1 + R^0_\parallel & 0 \end{pmatrix} \tag{A7}$$

$$\underline{\underline{T}}^0_6 = \begin{pmatrix} \left[1 - R^0_\parallel\right] \cos\theta^i_0 & 0 \\ 0 & -\left[1 + R^0_\perp\right] \end{pmatrix} \tag{A8}$$

Note that the matrices $\underline{\underline{T}}^0_5$ and $\underline{\underline{T}}^0_6$ originate from the expressions of the PO currents on the wedge. In analogous way, the matrix $\underline{\underline{T}}_n$ associated to S_n can be written as:

$$\underline{\underline{T}}_n = \underline{\underline{T}}_1 \left[\underline{\underline{T}}^n_2 \underline{\underline{T}}^n_4 \underline{\underline{T}}^n_5 + \underline{\underline{T}}^n_3 \underline{\underline{T}}^n_4 \underline{\underline{T}}^n_6 \right] \underline{\underline{T}}^n_7 \tag{A9}$$

$$\underline{\underline{T}}_2^n = \begin{pmatrix} 1-\sin^2\beta'\cos^2\phi & -\sin^2\beta'\sin\phi\cos\phi & -\cos\beta'\sin\beta'\cos\phi \\ -\sin^2\beta'\sin\phi\cos\phi & 1-\sin^2\beta'\sin^2\phi & -\cos\beta'\sin\beta'\sin\phi \\ -\cos\beta'\sin\beta'\cos\phi & -\cos\beta'\sin\beta'\sin\phi & \sin^2\beta' \end{pmatrix} \quad \text{(A10)}$$

$$\underline{\underline{T}}_3^n = \begin{pmatrix} 0 & \cos\beta' & -\sin\beta'\sin\phi \\ -\cos\beta' & 0 & \sin\beta'\cos\phi \\ \sin\beta'\sin\phi & -\sin\beta'\cos\phi & 0 \end{pmatrix} \quad \text{(A11)}$$

$$\underline{\underline{T}}_4^n = \frac{1}{\sqrt{1-\sin^2\beta'\sin^2(n\pi-\phi')}} \begin{pmatrix} \cos\beta'\cos n\pi & -\sin\beta'\cos n\pi\cos(n\pi-\phi') \\ cos\beta'\sin n\pi & -\sin\beta'\sin n\pi\cos(n\pi-\phi') \\ \sin\beta'\cos(n\pi-\phi') & \cos\beta' \end{pmatrix} \quad \text{(A12)}$$

$$\underline{\underline{T}}_5^n = \begin{pmatrix} 0 & [1-R_\perp^n]\cos\theta_n^i \\ 1+R_\parallel^n & 0 \end{pmatrix} \quad \text{(A13)}$$

$$\underline{\underline{T}}_6^n = \begin{pmatrix} \left[1-R_\parallel^n\right]\cos\theta_n^i & 0 \\ 0 & -[1+R_\perp^n] \end{pmatrix} \quad \text{(A14)}$$

$$\underline{\underline{T}}_7^n = \frac{1}{\sqrt{1-\sin^2\beta'\sin^2(n\pi-\phi')}} \begin{pmatrix} \cos\beta'\sin(n\pi-\phi') & -\cos(n\pi-\phi') \\ \cos(n\pi-\phi') & \cos\beta'\sin(n\pi-\phi') \end{pmatrix} \quad \text{(A15)}$$

REFERENCES

1. Tan, S. Y. and H. S. Tan, "UTD propagation model in an urban street scene for microcellular communications," *IEEE Trans. Electromagnetic Compat.*, Vol. 35, 423–428, 1993.
2. Erceg, V., A. J. Rustako, and R. S. Roman, "Diffraction around corners and its effect on the microcell coverage area in urban and suburban environments at 900 MHz, 2 GHz, and 6 GHz," *IEEE Trans. Veh. Technol.*, Vol. 43, 762–766, 1994.
3. Schuster, J. and R. Luebbers, "Hybrid SBR/GTD radio propagation model for site-specific predictions in an urban environment," *12th Ann. Rev. of Progress in Applied Computational Electromagnetics*, Vol. 1, 84–92, Monterey, CA, 1996.
4. Kanatas, A. G., I. D. Kountouris, G. B. Kostaras, and P. Constantinou, "A UTD propagation model in urban

microcellular environments," *IEEE Trans. Veh. Technol.*, Vol. 46, 185–193, 1997.

5. Rizk, K., J. F. Wagen, and F. Gardiol, "Two-dimensional ray-tracing modeling for propagation prediction in microcellular environments," *IEEE Trans. Veh. Technol.*, Vol. 46, 508–518, 1997.
6. Kanatas, A. G. and P. Constantinou, "A propagation prediction tool for urban mobile radio systems," *IEEE Trans. Veh. Technol.*, Vol. 49, 1348–1355, 2000.
7. Keller, J. B., "Geometrical theory of diffraction," *J. Opt. Soc. Amer.*, Vol. 52, 116–130, 1962.
8. Kouyoumjian, R. G. and P. H. Pathak, "A uniform geometrical theory of diffraction for an edge in a perfectly conducting surface," *Proc. IEEE*, Vol. 62, 1448–1461, 1974.
9. Luebbers, R. J., "Finite conductivity uniform GTD versus knife edge diffraction in prediction of propagation path loss," *IEEE Trans. Antennas Propagat.*, Vol. 32, 70–76, 1984.
10. Bernardi, P., R. Cicchetti, C. Gennarelli, G. Pelosi, and G. Riccio, "A UAPO solution for the field diffracted by building corners in wireless radio environments," *Antennas Wireless Propagat. Lett.*, Vol. 1, 169–172, 2002.
11. Taflove, A. and S. C. Hagness, *Computational Electrodynamics: The Finite-difference Time-domain Method*, Artech House, Norwood, 2000.
12. Senior, T. B. A. and J. L. Volakis, "Approximate boundary conditions in electromagnetics," *IEE Electromagnetic Waves Series*, London, 1995.
13. Yee, K. S., "Numerical solution of initial boundary value problems involving Maxwell's equations in isotropic media," *IEEE Trans. Antennas Propagat.*, Vol. 14, 302–307, 1966.
14. Gedney, S. D., "An anisotropic perfectly matched layer-absorbing medium for the truncation of FDTD lattices," *IEEE Trans. Antennas Propagat.*, Vol. 44, 1630–1639, 1996.